SHEP-12-29
July 15, 2014

Variations on a Higgs theme

S. Moretti

School of Physics and Astronomy, University of Southampton,

Highfield, Southampton SO17 1BJ, UK.

arXiv:1407.3511v1 [hep-ph] 13 Jul 2014

Abstract

We show how the Z boson can be generated in gluon-gluon fusion and yield two photons, via $gg \to Z \to \gamma\gamma$, through massive fermion loops only, thereby contributing events to a candidate Higgs sample in the di-photon channel. A sub-leading contribution also exists from $q\bar{q} \to Z \to \gamma\gamma$ events. Assuming the Standard Model, the corresponding event rates are negligible at the LHC stages of 7, 8 TeV, given the luminosities collected therein (about 5 and 20 fb^{-1}, respectively). Conversely, at 14 TeV, the first process become accessible for luminosities of order 300 fb^{-1}. Finally, we show how additional fermion states entering such loops, in production, in decay or in both cases, could affect the predictions in this channel by curiously mimicking Higgs signals.

1 Introduction

About a couple of years ago, the ATLAS and CMS experimental collaborations at the Large Hadron Collider (LHC) at CERN had announced the observation of a new boson, with a mass of about 125 GeV [1, 2], which was consistent with a Higgs particle, H, the last undiscovered object in the Standard Model (SM)[1]. The most recent results reported by ATLAS [5, 6] and CMS [7, 8, 9, 10] confirm such a Higgs boson discovery beyond doubt.

The decay channels investigated experimentally with highest precision are $H \to \gamma\gamma$, $H \to ZZ \to 4l$ and $H \to WW \to l\nu_l l^{(\prime)}\nu_{l^{(\prime)}}$, where $l^{(\prime)}$ denotes a lepton (electron and/or muon) and ν its associated neutrino. While these data are indeed compatible with the SM, they also indicate presently a small enhancement in the di-photon mode, with respect to SM. Indeed, the di-photon sample can be very sensitive to possible Beyond the SM (BSM) effects, owing to the fact that, amongst the aforementioned SM-like decay modes (or else the $b\bar{b}$ and $\tau^+\tau^-$ ones, to which ATLAS and CMS also have sensitivity, albeit reduced in comparison [11]), it is the only one in which such effects can enter at the same perturbative order as the SM ones, in the triangle loop connecting the Higgs boson to the two photons[2].

Fuelled by the fact that some analyses (at time with partial luminosity only) of di-photon data have seen over the past couple of years significant deviations from the SM predictions, a flurry of literature emerged trying to explain the latter in one or another BSM scenario. Far from endorsing either a SM or BSM hypothesis, we simply like to study here a forgotten contribution to the di-photon background which arises entirely in the SM. This is induced by $gg \to Z \to \gamma\gamma$, where the Z boson is never on mass-shell. In fact, contrary to a rather widespread popular belief in the community, following the detection of the $H \to \gamma\gamma$ decay mode, a spin-1 state can produce two photons, as the Landau-Yang theorem [12], often erroneously invoked, is actually only applicable to on-shell particles [13, 14]. (Similar arguments apply to the case of $gg \to Z$.) For the case of the Z boson of the SM, the coupling is induced in both $gg \to Z$ 'production' and $Z \to \gamma\gamma$ 'decay' solely via a triangle loop of heavy quarks (primarily the top one then) through the Goldstone component of the Z propagator (hence the effect is best seen in non-unitary gauges), which is in fact pseudoscalar in its couplings, hence in turn explaining why the W^+W^- loop does not enter the Z di-photon transition. We will compare the yield of the $gg \to Z \to \gamma\gamma$ and (also) $q\bar{q} \to Z \to \gamma\gamma$ processes against that of the SM Higgs process $gg \to H \to \gamma\gamma$ (occurring via two triangle loops, of quarks only in production and both bosons and fermions in decay) as well those of the customary backgrounds $gg \to \gamma\gamma$ (occurring via a box loop of quarks) and $q\bar{q} \to \gamma\gamma$ (occurring at tree level).

The plan of the paper is as follows. In the next section we describe the calculation. In the following one we discuss our results. We then conclude. We also have an appendix containing some key formulae.

[1] Some supplemental evidence was also gathered by CDF and D0 at FNAL [3, 4].

[2] A similar phenomenology also occurs in the $Z\gamma$ case, however, experimental sensitivity to this channel is much smaller with respect to the $\gamma\gamma$ case, so that only upper limits exist to date in this mode.

2 Calculation

Contrary to the claim made by hundreds of papers[3] stating that, if an excess is seen in the $\gamma\gamma$ decay channel, this cannot be produced by a spin-1 particle, we show here how this is possible. The very same papers often misleadingly quote the Landau-Yang's theorem [12], in order to support their claim. The latter, as originally formulated, is however only applicable to on-shell objects [13, 14] and is instead violated when, e.g., the $\gamma\gamma$ pair is produced by a Z boson which is not on-shell (i.e., non-resonant). Similar arguments can be applied to off-shell Z production via gg fusion. Therefore, the existence of the processes $gg \to Z \to \gamma\gamma$ and $q\bar{q} \to Z \to \gamma\gamma$ is perfectly legitimate. However, they can only occur through the pseudoscalar component of the (off-shell) Z boson: in other words, according to the Becchi-Stora-Rouet-Tyutin (BRST) [15] equalities, through its associated Goldstone component (in a generic R_ξ gauge)[4]. This is made evident if one uses the Landau gauge ($\xi \to 0$) for the calculation of the above process. The very fact that it is the pseudoscalar component of the Z boson to appear in it also means that in the $Z \to \gamma\gamma$ transition only fermion loops are involved, not (charged) gauge boson ones.

Two different calculations have been performed, so as to cross check one another. Furthermore, one computation was done analytically and the other numerically. In particular, the latter was done in the Landau gauge while the former in the unitary gauge. So, we are bound to use the unitary gauge ($\xi \to \infty$) to illustrate the calculation, which makes it more cumbersome yet more physically intuitive. But before doing so, let us list the inputs required to perform our numerical computations.

The relevant numerical inputs adopted here were as follows. For the top mass and width we have taken $m_t = 175$ GeV and $\Gamma_t = 1.55$ GeV, respectively. The Z mass used was $M_Z = 91.19$ GeV and was related to the W mass, M_W, via the SM formula $M_W = M_Z \cos\theta_W$, where $\sin^2\theta_W = 0.232$. (Corresponding widths were $\Gamma_Z = 2.5$ GeV and $\Gamma_W = 2.08$ GeV.) For the Higgs boson we have taken $M_H = 125$ GeV and $\Gamma_H = 4.2$ MeV. For the Electro-Magnetic (EM) coupling constant we have taken $\alpha = 1/128$ throughout. The Parton Distribution Functions (PDFs) that we have used are the CTEQ5L set [17] taken at the factorisation/renormalisation scale $Q = \mu = \sqrt{\hat{s}}$. (We also have checked other PDFs and adopted different scale choices, but found no significant difference in the relative size of the processes studied here.) The choice of PDFs dictates the running and parameters used to compute α_s. All rates are presented at the LHC energies of 7, 8 and 14 TeV[5].

[3] That we do not intend to quote here for obvious reasons, though a knowledgeable reader will be able to source these. We cite instead this paper [16], which also highlighted that this statement was wrong, though the solution proposed therein is different from ours, as the author illustrates possibly *resonant* $\gamma\gamma$ production through interference effects between a scalar and vector propagator, with suitable relative complex phase.

[4] Incidentally, the Goldstone of the Z originates in the Higgs doublet, hence it is not surprising that the Z boson can produce $\gamma\gamma$ pairs, just like the Higgs boson does.

[5] As we are only interested in the relative strenght of the aforementioned di-photon process, we do not include any strong or EW corrections in our analysis.

2.1 The computation of $gg \to Z \to \gamma\gamma$

We look first at the $Z \to \gamma\gamma$ transition and start with the following definitions:

- $p_1^\mu,\ p_2^\mu$ are the momenta of the two outgoing photons;
- $\epsilon_1^\mu,\ \epsilon_2^\mu$ are the polarisation vectors of the two outgoing photons;
- $q^\mu\,(= p_1^\mu + p_2^\mu)$ is the momentum of the incoming Z;
- ϵ_z^μ is the polarization vector of the Z.

The photons are on-shell and so we have

$$p_1 \cdot \epsilon_1 \ = \ p_2 \cdot \epsilon_2 \ = 0, \tag{1}$$

but the Z is off-shell and so we have

$$q \cdot \epsilon_z \ \neq \ 0. \tag{2}$$

We may in general expand the polarization vector of the Z as

$$\epsilon_z^\mu \ = \ \frac{\epsilon_z \cdot q}{q^2} q^\mu - \epsilon_z \cdot \epsilon_1^* \epsilon_1^\mu - \epsilon_z \cdot \epsilon_2^* \epsilon_2^\mu - \frac{\epsilon_z \cdot (p_1 - p_2)}{q^2} \left(p_1^\mu - p_2^\mu\right). \tag{3}$$

The relation in unitary gauge

$$\sum_\lambda \epsilon_z^\mu(\lambda)\epsilon^\nu(\lambda) \ = \ -g^{\mu\nu} + \frac{q^\mu q^\nu}{M_Z^2} \tag{4}$$

leads to

$$\epsilon_z \cdot q \ = \ \sqrt{\frac{q^2}{M_Z^2}(q^2 - M_Z^2)}. \tag{5}$$

This vanishes when the Z goes on shell (as expected).

If we allow the matrix element for the vertex $Z \to \gamma\gamma$ to be a vector with index μ we do not need to discuss the polarisation vector of the Z. We show that this vertex is proportional to q^μ where q is the momentum of the Z.

The amplitude (wherein the helical lines represent either photons or gluons whereas the wavy line refers to the Z)

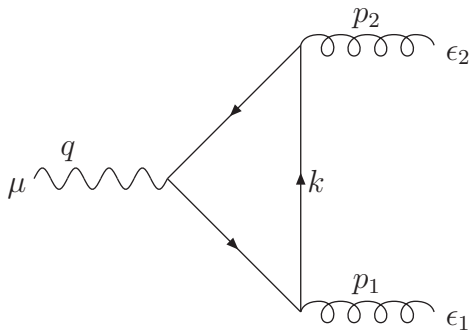

is not gauge invariant for an off-shell Z and we work in the gauge

$$p_2 \cdot \epsilon_1 \;=\; p_1 \cdot \epsilon_2 \;= 0. \tag{6}$$

Such an amplitude is given by (wherein m is the fermion mass)

$$\mathcal{A} \;=\; e^2 C_A \int \frac{d^4k}{(2\pi)^4} \frac{(\mathcal{N}_1 + \mathcal{N}_2)}{(k^2 - m^2)((k-p_2)^2 - m^2)((k+p_1)^2 - m^2)} \tag{7}$$

where

$$\mathcal{N}_1 \;=\; \mathrm{Tr}\left(\gamma \cdot \epsilon_1 (\gamma \cdot k + m)(\gamma \cdot (k - p_2) + m)\gamma^\mu \left(g_V + g_A \gamma^5\right)(\gamma \cdot (k + p_1) + m)\right) \tag{8}$$

from the graph shown and

$$\mathcal{N}_2 \;=\; -\mathrm{Tr}\left(\gamma \cdot \epsilon_1 (\gamma \cdot (k + p_1) - m)\gamma^\mu \left(g_V + g_A \gamma^5\right)(\gamma \cdot (k - p_2) - m)\gamma \cdot \epsilon_2 (\gamma \cdot k - m)\right) \tag{9}$$

from the graph with the fermions circulating in the reverse direction. The factor of $C_A (= 3)$ comes from summing over all colours of internal quarks.

These terms are written in terms of the Passarino-Veltman [18] functions defined in the usual way. In the case of equal masses we have the following relations:

a.

$$B_1(q^2, m^2, m^2) \;=\; -\frac{1}{2} B_0(q^2, m^2, m^2)$$

b.

$$C_{11}(0, q^2, 0, m^2, m^2, m^2) \;=\; \frac{2}{q^2} B_0(q^2, m^2, m^2)$$

c.

$$C_{12}(0, q^2, 0, m^2, m^2, m^2) \;=\; \frac{1}{q^2} B_0(q^2, m^2, m^2)$$

d.

$$4C_{24}(0, q^2, 0, m^2, m^2, m^2) \;=\; 1 + B_0(q^2, m^2, m^2) + 2m^2 C_0(0, q^2, 0, m^2, m^2, m^2)$$

e.

$$C_{21}(0, q^2, 0, m^2, m^2, m^2) \;=\; \frac{1}{q^2}\left(1 - B_0(q^2, m^2, m^2) + 2m^2 C_0(0, q^2, 0, m^2, m^2, m^2)\right)$$

f.

$$C_{22}(0, q^2, 0, m^2, m^2, m^2) \;=\; -\frac{1}{2q^2} B_0(q^2, m^2, m^2)$$

g.

$$C_{23}(0,q^2,0,m^2,m^2,m^2) \;=\; \frac{1}{2q^2}\left(1-B_0(q^2,m^2,m^2)+2m^2C_0(0,q^2,0,m^2,m^2,m^2)\right)$$

so that everything can be expressed in terms of two master integrals:

$$B_0(q^2,m^2,m^2) \;=\; -\int_0^1 d\alpha \ln\left(1-\frac{s\alpha(1-\alpha)}{m^2}\right) \tag{10}$$

and

$$C_0(0,q^2,0,m^2,m^2,m^2) \;=\; \int_0^1 \frac{d\alpha}{\alpha}\ln\left(1-\frac{s\alpha(1-\alpha)}{m^2}\right). \tag{11}$$

These two integrals can in turn be expressed in terms of logarithms and di-logarithms, as seen in the appendix.

Taking the trace, applying the above relations and developing the kinematics, we find (after some manipulations carried out using FORM [19]) the following relation:

$$\mathcal{A} \;=\; \frac{\alpha}{\pi}g_A C_A\left[\frac{q^\mu}{q^2}\epsilon_{\sigma\nu\rho\tau}p_1^\sigma p_2^\nu\epsilon_1^\rho\epsilon_2^\tau\left(B_0-1-2m^2C_0\right)+\frac{1}{2}\epsilon_{\sigma\nu\rho}{}^\mu(p_1-p_2)^\sigma\epsilon_1^\nu\epsilon_2^\rho\left(1-B_0-2m^2C_0\right)\right]. \tag{12}$$

We remark here that, as expected, the amplitude is proportional to g_A, the axial coupling of he Z to fermions. In fact, for the vector coupling, the amplitude vanishes identically by Furry's theorem [20].

Now we note that

$$\epsilon_{\sigma\nu\rho\tau}p_1^\sigma p_2^\nu\epsilon_1^\rho\epsilon_2^\tau \;=\; \frac{1}{2}\epsilon_{\sigma\nu\rho\tau}(p_1-p_2)^\sigma(p_1+p_2)^\nu\epsilon_1^\rho\epsilon_2^\tau \tag{13}$$

and, since $p_1,p_2,\epsilon_1,\epsilon_2$ are mutually orthogonal ($s=(p_1+p_2)^2$),

$$\epsilon_{\sigma\nu\rho}{}^\mu(p_1-p_2)^\sigma\epsilon_1^\nu\epsilon_2^\rho \;=\; \frac{q^\mu}{s}\epsilon_{\sigma\nu\rho\tau}(p_1-p_2)^\sigma(p_1+p_2)^\nu\epsilon_1^\rho\epsilon_2^\tau. \tag{14}$$

This amplitude is thus reduced to

$$\mathcal{A} \;=\; -2\frac{q^\mu}{s}\frac{\alpha}{\pi}g_A m^2 C_0 C_A\epsilon_{\sigma\nu\rho\tau}(p_1-p_2)^\sigma(p_1+p_2)^\nu\epsilon_1^\rho\epsilon_2^\tau. \tag{15}$$

We also have a similar term from the production vertex from gluon-gluon scattering with α replaced by α_s and the colour factor C_A replaced by $\frac{1}{2}\delta_{ab}$ (a,b are the gluon colours).

The full amplitude for the process

$$g(p_1,\lambda_1)+g(p_2,\lambda_2) \;\to\; Z \;\to\; \gamma(p_3,\lambda_3)+\gamma(p_4,\lambda_4)$$

is therefore given by

$$\begin{aligned}\mathcal{A} &= 4C_A\delta_{ab}\frac{\alpha\alpha_s}{s^2\pi^2}\sum_{i,j} g_A^{(i)}g_A^{(j)}\, m_i^2 m_j^2\, C_0(0,s,0,m_i^2,m_i^2,m_i^2)\, C_0(0,s,0,m_j^2,m_j^2,m_j^2) \\ &\times\ [\epsilon_{\sigma\nu\rho\tau}(p_1-p_2)^\sigma(p_1+p_2)^\nu\epsilon_1^\rho\epsilon_2^\tau]\left[\epsilon_{\sigma'\nu'\rho'\tau'}(p_3-p_4)^{\sigma'}(p_3+p_4)^{\nu'}\epsilon_3^{\rho'}\epsilon_4^{\tau'}\right] \\ &\times q^\alpha q^\beta\left(\frac{g_{\alpha\beta}-\frac{q_\alpha q_\beta}{M_Z^2}}{(s-M_Z^2)}\right)\end{aligned}$$

where the $\sum_{i,j}$ goes over all flavours of internal quarks and is dominated by the top one (the contribution from lepton loops in the Z decay being negligible).

Now,

$$q^\alpha q^\beta\left(g_{\alpha\beta}-\frac{q_\alpha q_\beta}{M_Z^2}\right) \;=\; s-\frac{s^2}{M_Z^2}, \tag{16}$$

so we see that the Z-pole cancels and we get

$$\begin{aligned}\mathcal{A} &= 4C_A\delta_{ab}\frac{\alpha\alpha_s}{M_Z^2 s\pi^2}\sum_{i,j} g_A^{(i)}g_A^{(j)}\, m_i^2 m_j^2\, C_0(0,s,0,m_i^2,m_i^2,m_i^2)\, C_0(0,s,0,m_j^2,m_j^2,m_j^2) \\ &\times\ [\epsilon_{\sigma\nu\rho\tau}(p_1-p_2)^\sigma(p_1+p_2)^\nu\epsilon_1^\rho\epsilon_2^\tau]\left[\epsilon_{\sigma'\nu'\rho'\tau'}(p_3-p_4)^{\sigma'}(p_3+p_4)^{\nu'}\epsilon_3^{\rho'}\epsilon_4^{\tau'}\right].\end{aligned}$$

2.2 The computation of $q\bar{q}\to Z\to\gamma\gamma$

For the process

$$q\,\bar{q}\;\to\;Z\;\to\;\gamma\,\gamma$$

the vertex representing gluon-gluon fusion is replaced by the coupling of the Z to the incoming quarks,

$$\overline{v}(\lambda_1,p_1)\gamma^\mu\left(g_v-g_A\gamma^5\right)u(\lambda_2,p_2). \tag{17}$$

The vertex from the Z decay still projects out the polarisation proportional to q^μ and so we may rewrite this (after the projection) as (m is the quark mass)

$$\frac{q^\mu q^\nu}{s}\overline{v}(\lambda_1,p_1)\gamma^\nu(g_v-g_A\gamma^5)u(\lambda_2,p_2) \;=\; \frac{q^\mu}{s}g_A 2m\overline{v}(\lambda_1,p_1)\gamma^5 u(\lambda_2,p_2) \;=\; \frac{q^\mu}{\sqrt{s}}g_A 2m\delta_{\lambda_1,-\lambda_2} \tag{18}$$

using

$$\overline{v}(\lambda_1,p_1)\gamma^5 u(\lambda_2,p_2) \;=\; \sqrt{2p_1\cdot p_2}\,\delta_{\lambda_1,-\lambda_2}, \tag{19}$$

for massless fermions.

Thus the amplitude from the process with incoming quark-antiquark pairs of mass m_i and colours i,j is

$$\mathcal{A} \;=\; 4C_A\delta_{ij}\delta_{\lambda_1,-\lambda_2}\frac{\alpha}{M_Z^2\sqrt{s}\pi}m_i g_A^{(i)}\sum_j g_A^{(j)}\, m_j^2\, C_0(0,s,0,m_j^2,m_j^2,m_j^2)\epsilon_{\sigma'\nu'\rho'\tau'}(p_3-p_4)^{\sigma'}(p_3+p_4)^{\nu'}\epsilon_3^{\rho'}\epsilon_4^{\tau'}. \tag{20}$$

Furthermore, we have the relations

$$\epsilon_{\sigma'\nu'\rho'\tau'}(p_3-p_4)^{\sigma'}(p_3+p_4)^{\nu'}\epsilon_3^{\rho'}\epsilon_4^{\tau'} \;=\; s\delta_{\lambda_3,\lambda_4} \tag{21}$$

and

$$m_j^2\, C_0(0,s,0,m_j^2,m_j^2,m_j^2) \;=\; -2f\left(\frac{4m_j^2}{s}\right) \tag{22}$$

with $f(\tau)$ as in, e.g., Ref. [21].

Therefore

$$\mathcal{A} \;=\; -8C_A\delta_{ij}\delta_{\lambda_1,-\lambda_2}\frac{\alpha\sqrt{s}}{M_Z^2\pi}m_i g_A^{(i)}\sum_j g_A^{(j)}\, f\left(\frac{4m_j^2}{s}\right)\,\delta_{\lambda_3,\lambda_4}. \tag{23}$$

Also (here $g_W = e/\sin\theta_W$),

$$\frac{g_A}{M_Z} \;=\; \pm\frac{1}{2}\frac{g_W}{M_W} \tag{24}$$

and so we have finally

$$\mathcal{A} \;=\; \pm 2\frac{g_W^2}{M_W^2}C_A\delta_{ij}\delta_{\lambda_1,-\lambda_2}\frac{\alpha\sqrt{s}}{\pi}m_i\sum_j(-1)^j\, f\left(\frac{4m_j^2}{s}\right)\,\delta_{\lambda_3,\lambda_4}. \tag{25}$$

Note the δ-functions for *both* the incoming quark helicities (which must be opposite since the mass insertion requires helicity flip) and the outgoing photons (which must have the same helicity to conserve angular momentum).

3 Results

The total (inclusive) cross sections (in fb) for the processes $gg \to Z \to \gamma\gamma$ and $q\bar{q} \to Z \to \gamma\gamma$ at the LHC with $\sqrt{s} = 7, 8$ and 14 TeV is found in Tab. 3. Given the accumulated luminosities at the first two stages of the LHC, 5 (at 7 TeV) and 20 (at 8 TeV) fb^{-1}, it is clear that neither of the processes is accessible therein. In contrast, at the highest energy stage (i.e., 14 TeV) with design luminosity (say, 300 fb^{-1}), one should expect some 17 events from gg fusion and again none from $q\bar{q}$ scatterings, at inclusive level. If the typical SM Higgs selection cuts

$$p_\gamma^T > 20 \text{ GeV}, \quad |\eta_\gamma| < 2.5, \quad M_{\gamma\gamma} > 100 \text{ GeV}, \tag{26}$$

in transverse momentum (p^T), pseudorapidity (η) and invariant mass ($M_{\gamma\gamma}$) of the photons, are enforced, then the detectable events (at $\sqrt{s} = 14$ TeV with $\mathcal{L}dt = 300$ fb^{-1} for the gg case) scale down to 10.

These are rather small numbers and, if regarded as contributors to a candidate Higgs sample at the LHC (again, with design energy and luminosity), they are very subleading with respect to both the $gg \to H \to \gamma\gamma$ signal (yielding 47 fb after the cuts in eq. (26) and

the other known background in the gg channel, i.e., $gg \to Box \to \gamma\gamma$ (giving 793 fb after cuts). In fact, it should be noted that the dominant di-photon background is the tree-level $q\bar{q} \to \gamma\gamma$, as it produces 6770 fb of cross section (after cuts). In the light of these results, we will then neglect from now on discussion of the $q\bar{q} \to Z \to \gamma\gamma$ process, apart from a reference histogram in the upcoming figure[6].

The differential distributions in the di-photon invariant mass for the two processes under consideration, $gg \to Z \to \gamma\gamma$ and $q\bar{q} \to Z \to \gamma\gamma$, at 14 TeV, are found in Fig. 1. This shows that much of the cross section is located around the top-antitop threshold, $M_{\gamma\gamma} \approx 2m_t$, for both channels. This confirms, as expected, the dominance of the top contribution in the triangle loops. Furthermore, notice that the increase at threshold is more pronounced for the gg subchannel, in comparison to the $q\bar{q}$ one, owing to the fact that the aforementioned loop appears both in production and decay for $gg \to Z \to \gamma\gamma$ whereas only in decay for $q\bar{q} \to Z \to \gamma\gamma$. This pattern is the same before and after the cuts in eq. (26).

Fig. 2 illustrates again the subdominance of the $gg \to Z \to \gamma\gamma$ process with respect to the others mentioned above, i.e., $gg \to H \to \gamma\gamma$, $gg \to Box \to \gamma\gamma$ and $q\bar{q} \to \gamma\gamma$, now seen in the di-photon invariant mass. This is shown after the aforementioned cuts. Yet, with increasing di-photon invariant masses, up to around $2m_t$ and onwards, the relative importance of $gg \to Z \to \gamma\gamma$ with respect to the other channels grows steadily, reaching in such an invariant mass region the 0.2 permille level with respect to the leading $q\bar{q} \to \gamma\gamma$ term. (Notice that the curves are obtained from a fit to histograms which are 10 GeV wide, hence the distorted shape of the (otherwise very narrow) H peak.)

The $gg \to Z \to \gamma\gamma$ channel becomes relatively more important, with respect to the other di-photon backgrounds, if viewed differentially, in the polar angle of either of the photons, θ, when defined in the rest frame of the Center-of-Mass (CM). This observable, as it is well known, is sensitive to both the spin and CP-properties of the Higgs boson and it has been extensively used for this purpose by the ATLAS and CMS collaborations (see, e.g., Ref. [22]). By looking at Fig. 3, it is clear that, while the $gg \to Box \to \gamma\gamma$ and $q\bar{q} \to \gamma\gamma$ backgrounds have a completely different structure in $\cos\theta$ with respect to the $gg \to H \to \gamma\gamma$ signal, the shape of $gg \to Z \to \gamma\gamma$ is very similar to it. Hence, in this observable more than others, one ought to achieve an accurate modelling of the complete background, including the contribution from the gg process that we have computed here.

Before closing, we would also like to emphasise that the $gg \to Z \to \gamma\gamma$ process, in virtue of its loop structure that is doubly sensitive to virtual heavy (coloured) fermions (i.e., both in production and decay), can in principle reveal the presence of additional states of this kind, with respect to the SM, which may or may not be accessible via direct searches. Fig. 4 illustrates this for the case of, e.g., one additional generation of up- and -down-type vector-like quarks[7], with both standard ($+2/3$ and $-1/3$, respectively) and exotic ($+5/3$ and $-4/3$, respectively) EM charges, both cases with masses 700 (up-type) and 500 (down-type) GeV. (These states are predicted by various theoretical frameworks like, e.g., composite Higgs

[6]We have also investigated possible interference effects between the $q\bar{q} \to Z \to \gamma\gamma$ amplitude and the $q\bar{q} \to \gamma\gamma$ one and found them negligible.

[7]Notice that the presence of a possible fourth generation of SM-type fermions is less and less favourite by the LHC Higgs data, see [23] for a review.

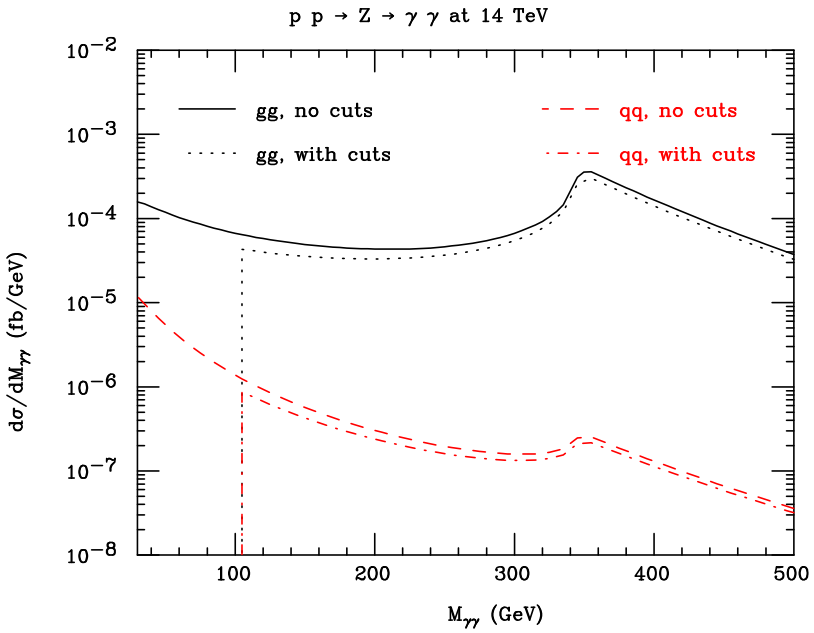

Figure 1: Differential di-photon mass distributions at the 14 TeV LHC for the processes $gg \to Z \to \gamma\gamma$ and $q\bar{q} \to Z \to \gamma\gamma$ before and after the cuts $p_\gamma^T > 20$ GeV, $|\eta_\gamma| < 2.5$ and $M_{\gamma\gamma} > 100$ GeV. CTEQ(5L) with $Q = \mu = \sqrt{\hat{s}}$ is used.

models[8], little Higgs models, scenarios with extra dimensions, models with gauging of the flavour group, non-minimal supersymmetric extensions as well as Grand Unified Theories.) As expected, we notice in the plotted spectra the additional thresholds at (twice) the above two masses[9].

$gg \to Z \to \gamma\gamma$

	7 TeV	8 TeV	14 TeV
Before cuts	0.014	0.018	0.055
After cuts	0.0067	0.0095	0.034

$q\bar{q} \to Z \to \gamma\gamma$

	7 TeV	8 TeV	14 TeV
Before cuts	0.00045	0.00053	0.0010
After cuts	2.21×10^{-5}	2.95×10^{-5}	9.02×10^{-5}

Table 1: Cross section in fb for $gg \to Z \to \gamma\gamma$ and $q\bar{q} \to Z \to \gamma\gamma$ at the three LHC energy stages. The selection enforced employs the following cuts: $p_\gamma^T > 20$ GeV, $|\eta_\gamma| < 2.5$ and $M_{\gamma\gamma} > 100$ GeV. CTEQ(5L) with $Q = \mu = \sqrt{\hat{s}}$ is used.

[8]Our chosen illustrative case is from the so-called 4-Dimensional Composite Higgs Model (4DCHM) of Ref. [24], as implemented in [25], wherein the above masses are consistent with experiment [26].

[9]Despite the fact that one cannot and will not be able to reconstruct the Breit-Wigner shaped 'Higgs resonance' from data, owing to the fact that the Higgs boson of the SM is 4.2 MeV wide at 125 GeV and the di-photon mass resolution of detectors is and will remain far larger than this, so that data actually shape a Gaussian 'Higgs enhancement', we find it of very speculative value and of little phenomenological relevance, at least to our judgment, to mention here that a 62.5 GeV fermion could actually easily conspire to produce a 125 GeV 'threshold enhancement', very nearly Gaussian in shape.

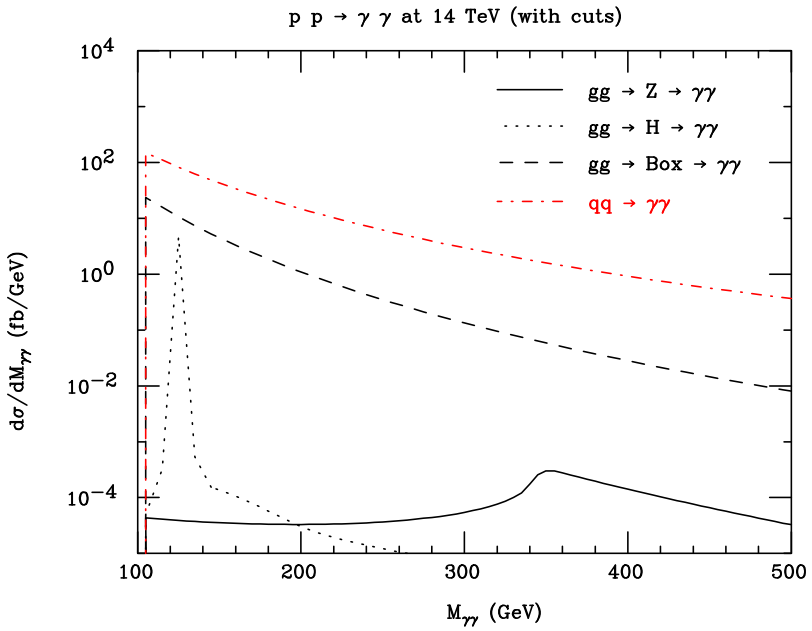

Figure 2: Differential di-photon mass distributions at the 14 TeV LHC for the processes $gg \to Z \to \gamma\gamma$, $gg \to H \to \gamma\gamma$, $gg \to Box \to \gamma\gamma$ and $q\bar{q} \to \gamma\gamma$ after the cuts $p_\gamma^T > 20$ GeV, $|\eta_\gamma| < 2.5$ and $M_{\gamma\gamma} > 100$ GeV. CTEQ(5L) with $Q = \mu = \sqrt{\hat{s}}$ is used.

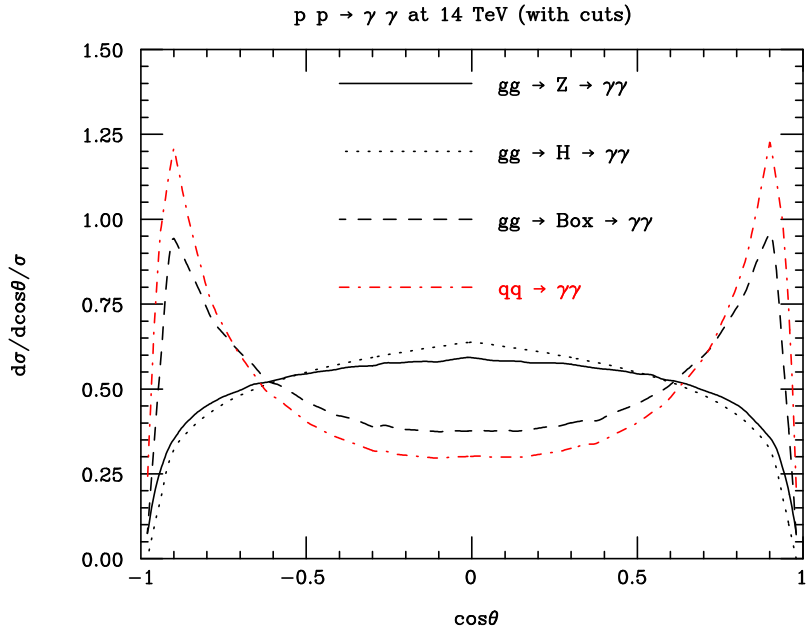

Figure 3: Differential polar angle (defined in the CM rest frame) distributions at the 14 TeV LHC for the processes $gg \to Z \to \gamma\gamma$, $gg \to H \to \gamma\gamma$, $gg \to Box \to \gamma\gamma$ and $q\bar{q} \to \gamma\gamma$ after the cuts $p_\gamma^T > 20$ GeV, $|\eta_\gamma| < 2.5$ and $M_{\gamma\gamma} > 100$ GeV. CTEQ(5L) with $Q = \mu = \sqrt{\hat{s}}$ is used. Note the normalisation to unity.

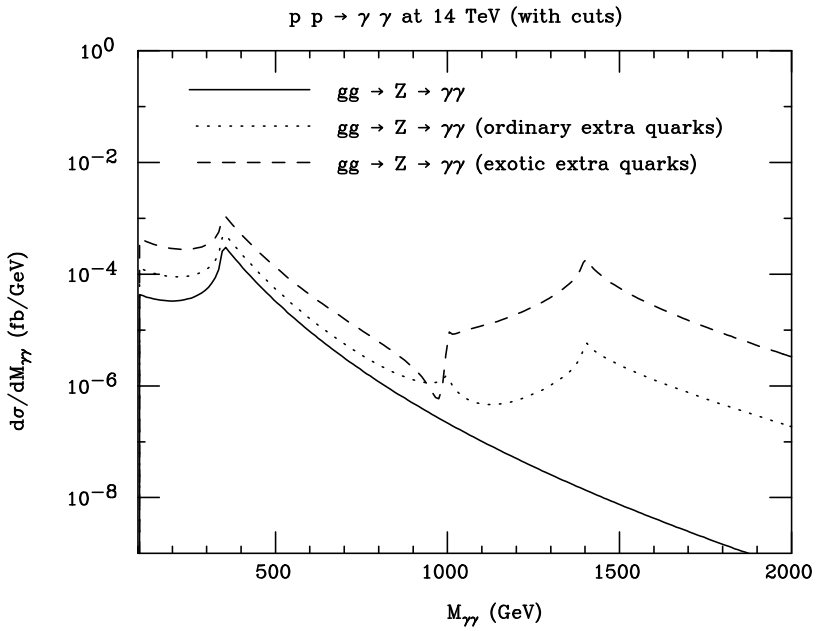

Figure 4: Differential di-photon mass distributions at the 14 TeV LHC for the processes $gg \to Z \to \gamma\gamma$, $gg \to Z \to \gamma\gamma$ including one additional generation of ordinary quarks $gg \to Z \to \gamma\gamma$ including one additional generation of exotic quarks after the cuts $p_\gamma^T > 20$ GeV, $|\eta_\gamma| < 2.5$ and $M_{\gamma\gamma} > 100$ GeV. CTEQ(5L) with $Q = \mu = \sqrt{\hat{s}}$ is used.

4 Conclusions

We have studied the yield of the two processes $gg \to Z \to \gamma\gamma$ and $q\bar{q} \to Z \to \gamma\gamma$ in the SM at the LHC. These two channels emerge only when the intermediate Z boson is off-shell, so that they are never large, though the gg subchannel can be accessed at the CERN machine with 14 GeV and luminosities of order 300 fb^{-1} unlike the $q\bar{q}$ mode which will remain unobserved. While never competitive in size with the di-photon Higgs sample or the already known di-photon backgrounds, they may have to eventually be accounted for in high precision measurements, particularly because the spin and CP-properties reconstructed from the two photons in our reference gg-induced process are very similar to those of the Higgs signal, thus differently from the case of the other backgrounds. Finally, we have shown the sensitivity of this channel to the certain presence of the top quark and the possibile one of additional heavy vector-like quarks (as an illustrative example) entering in the loops.

In the longer term, the new channels studied here may also become quite significant in size, for example, after a few years of running at the so-called Super-LHC, a tenfold increase in istantaneous luminosity of the standard 14 TeV LHC [27], which is currently being considered.

In summary, we have performed this calculation for the mere purpose of quantifying all possible sources of di-photon events from the SM, no matter how small they could be, especially in presence of unsettled di-photon data measurements. After all, recall that the 125 GeV Higgs discovery was claimed on the basis of very few events, many from $\gamma\gamma$, so one

would want that another Higgs boson is erroneously 'discovered' in the di-photon channel with apparent mass at 350 GeV (or elsewhere) in a few years from now.

Acknowledgments

SM is supported in part through the NExT Institute. He is grateful to D.A. Ross for double-checking the calculation, providing analytical formulae and innumerable useful comments on the analysis. We also acknowledge useful discussions with E. Accomando.

References

[1] ATLAS Collaboration, Phys. Lett. B716 (2012) 1 [arXiv:1207.7214 [hep-ex]].

[2] CMS Collaboration, Phys. Lett. B716 (2012) 30 [arXiv:1207.7235 [hep-ex].

[3] CDF and D0 Collaborations, Phys. Rev. Lett. 109 (2012) 071804 [arXiv:1207.6436 [hep-ex]].

[4] CDF and D0 Collaborations, Phys. Rev. D88 (2013) 052014 [arXiv:1303.6346 [hep-ex]].

[5] ATLAS Collaboration, CERN preprint ATLAS-CONF-2013-034.

[6] ATLAS Collaboration, CERN preprint ATLAS-CONF-2013-072.

[7] CMS Collaboration, Phys. Lett. B726 (2013) 587 [arXiv:1307.5515].

[8] CMS Collaboration, arXiv:1310.1002 [hep-ex].

[9] CMS Collaboration, CERN preprint CMS-PAS-HIG-13-005 (2013).

[10] CMS Collaboration, arXiv:1407.0558 [hep-ex].

[11] ATLAS Collaboration, CERN preprint ATLAS-CONF-2013-108;
ATLAS Collaboration, CERN preprint ATLAS-CONF-2014-009;
CMS Collaboration, Nature Physics (2014);
CMS Collaboration, Phys. Rev. D89 (2014) 012003 [arXiv:1310.3687 [hep-ex]];
CMS Collaboration, JHEP 05 (2014) 104 [arXiv:1401.5041 [hep-ex]].

[12] L.D. Landau, Dokl. Akad. Nauk SSSR 60 (1948) 207;
C.N. Yang, Phys. Rev. 77 (1950) 242.

[13] E.V. Zhemchugov, arXiv:1402.1203 [hep-ph].

[14] N. Kanda, R. Abe, T. Fujita, H. Kato and H. Tsuda, arXiv:1109.0926 [hep-ph].

[15] C. Becchi, A. Rouet and R. Stora, Phys. Lett. B52, 344 (1974), Commun. Math. Phys. 42, 127 (1975) and Ann. Phys. 98, 2 (1976);
I.V. Tyutin, arXiv:0812.0580 [hep-th].

[16] J. P. Ralston, arXiv:1211.2288 [hep-ph].

[17] H. L. Lai, J. Huston, S. Kuhlmann, J. Morfin, F. Olness, J. F. Owens, J. Pumplin and W. K. Tung, Eur. Phys. J. C12 (2000) 375 [arXiv:hep-ph/9903282].

[18] G. Passarino and M.J.G. Veltman, Nucl. Phys. B160 (1979) 151.

[19] J.A.M. Vermaseren, arXiv:math-ph/0010025.

[20] W.H. Furry, Phys. Rev. 51 (1937) 125;
R. P. Feynman, Phys. Rev. 76 (1949) 749;
F. J. Dyson, Phys. Rev. 75 (1949) 1736.

[21] J.F. Gunion, H.E. Haber, G.L. Kane and S. Dawson, *The Higgs Hunter's Guide*, Addison-Wesley, Reading MA 1990.

[22] ATLAS Collaboration, Phys. Lett. B726 (2013) 120 [arXiv:1307.1432 [hep-ex]] and CERN preprint ATLAS-CONF-2013-040; CMS Collaboration, arXiv:1212.6639 [hep-ex]

[23] A. Lenz, Adv. High Energy Phys. 2013 (2013) 910275 (and references therein).

[24] S. De Curtis, M. Redi and A. Tesi, JHEP 04 (2012) 042 [arXiv:1110.1613 [hep-ph]].

[25] D. Barducci, A. Belyaev, M. S. Brown, S. De Curtis, S. Moretti and G. M. Pruna, JHEP 09 (2013) 047 [arXiv:1302.2371 [hep-ph]].

[26] D. Barducci, A. Belyaev, M. Buchkremer, G. Cacciapaglia, A. Deandrea, S. De Curtis, J. Marrouche and S. Moretti *et al.*, arXiv:1405.0737 [hep-ph] (and references therein).

[27] F. Gianotti, M. L. Mangano, T. Virdee *et al.*, Eur. Phys. J. C39 (2005) 293 [arXiv:hep-ph/0204087].

Appendix: calculation of the integrals C_0 and B_0

We start with

$$C_0(s,m^2) \;\equiv\; -i\int \frac{d^4k}{\pi^2}\frac{1}{(k^2-m^2)((k-p_1)^2-m^2)((k+p_2)^2-m^2)}, \tag{27}$$

where $p_1^2 = p_2^2 = 0$ and $2p_1\cdot p_2 = s$.

Upon Feynman parameterisation and by shifting the loop momentum to $k + p_1\alpha - p_2\beta$, one has

$$C_0 \;=\; -2i\int \frac{d^4k}{\pi^2}\int_0^1 d\alpha d\beta\theta(1-\alpha-\beta)\frac{1}{\left[k^2+s\alpha\beta-m^2\right]^3}. \tag{28}$$

Performing the loop integral, we get

$$C_0 \;=\; \int_0^1 d\alpha d\beta\theta(1-\alpha-\beta)\frac{1}{\left[s\alpha\beta-m^2\right]}. \tag{29}$$

Integrating over β gives

$$C_0 \;=\; \frac{1}{s}\int_0^1 \frac{d\alpha}{\alpha}\ln\left(1-\frac{s\alpha(1-\alpha)}{m^2}\right). \tag{30}$$

Defining

$$\tau \;\equiv\; \frac{4m^2}{s} \tag{31}$$

gives

$$C_0 \;=\; \frac{1}{s}\int_0^1 \frac{d\alpha}{\alpha}\ln\left(1-\frac{4\alpha(1-\alpha)}{\tau}\right). \tag{32}$$

Factorising the argument of the logarithm produces

$$C_0 \;=\; \frac{1}{s}\int_0^1 \frac{d\alpha}{\alpha}\left[\ln\left(1-\frac{2\alpha}{1+\sqrt{1-\tau}}\right)+\ln\left(1-\frac{2\alpha}{1-\sqrt{1-\tau}}\right)\right] \tag{33}$$

where we assume here that $\tau < 1$ so that we are above threshold (i.e., we will have an imaginary part).

Then change variables to

$$\beta_1 \;=\; \frac{2\alpha}{1+\sqrt{1-\tau}} \tag{34}$$

for the first term and

$$\beta_2 \;=\; \frac{2\alpha}{1-\sqrt{1-\tau}} \tag{35}$$

for the second term to get

$$\begin{aligned} C_0 &= \frac{1}{s}\left[\int_0^{2/(1+\sqrt{1-\tau})} \frac{d\beta_1 \ln(1-\beta_1)}{\beta_1} + \int_0^{2/(1-\sqrt{1-\tau})} \frac{d\beta_2 \ln(1-\beta_2)}{\beta_2}\right] \\ &= \frac{1}{s}\left[-\frac{\pi^2}{3} + \int_1^{2/(1+\sqrt{1-\tau})} \frac{d\beta_1 \ln(1-\beta_1)}{\beta_1} + \int_1^{2/(1-\sqrt{1-\tau})} \frac{d\beta_2 \ln(1-\beta_2)}{\beta_2}\right]. \end{aligned}$$

Now change again variables to $\gamma_i \equiv \frac{1}{\beta_i}$ $(i = 1, 2)$ to get

$$\begin{aligned} C_0 &= \frac{1}{s}\left[-\frac{\pi^2}{3} - \int_1^{(1+\sqrt{1-\tau})/2} \frac{d\gamma_1}{\gamma_1} \ln\left(1-\frac{1}{\gamma_1}\right) - \int_1^{(1-\sqrt{1-\tau})/2} \frac{d\gamma_2}{\gamma_2} \ln\left(1-\frac{1}{\gamma_2}\right)\right] \\ &= \frac{1}{s}\left[-\frac{\pi^2}{3} - \int_1^{(1+\sqrt{1-\tau})/2} \frac{d\gamma_1}{\gamma_1} \left(\ln\left(1-\gamma_1\right)) - \ln(-\gamma_1)\right) - \int_1^{(1-\sqrt{1-\tau})/2} \frac{d\gamma_2}{\gamma_2} \left(\ln\left(1-\gamma_2\right)) - \ln(-\gamma_2)\right)\right] \\ &= \frac{1}{s}\left[-\frac{\pi^2}{3} + \frac{1}{2}\ln^2\left(\frac{1+\sqrt{1-\tau}}{2}\right) - i\pi\left|\ln\left(\frac{1+\sqrt{1-\tau}}{2}\right)\right|\right. \\ &\quad + \frac{1}{2}\ln^2\left(\frac{1-\sqrt{1-\tau}}{2}\right) - i\pi\left|\ln\left(\frac{1-\sqrt{1-\tau}}{2}\right)\right| \\ &\quad \left. - \int_1^{(1+\sqrt{1-\tau})/2} \frac{d\gamma_1}{\gamma_1} \ln\left(1-\gamma_1\right) - \int_1^{(1-\sqrt{1-\tau})/2} \frac{d\gamma_2}{\gamma_2} \ln\left(1-\gamma_2\right)\right], \end{aligned} \tag{36}$$

where the sign of the imaginary part has been set to be negative as required by unitarity.

Now we integrate the final term in (36) by parts and rename the variable of integration $\gamma_2 \to 1-\gamma_1$ to achieve

$$\begin{aligned} C_0 &= \frac{1}{s}\left[-\frac{\pi^2}{3} + \frac{1}{2}\ln^2\left(\frac{1+\sqrt{1-\tau}}{2}\right) \pm i\pi \ln\left(\frac{1+\sqrt{1-\tau}}{2}\right)\right. \\ &\quad + \frac{1}{2}\ln^2\left(\frac{1-\sqrt{1-\tau}}{2}\right) \pm i\pi \ln\left(\frac{1-\sqrt{1-\tau}}{2}\right) \\ &\quad - \int_1^{(1+\sqrt{1-\tau})/2} \frac{d\gamma_1}{\gamma_1} \ln\left(1-\gamma_1\right) + \int_0^{(1+\sqrt{1+\tau})/2} \frac{d\gamma_1}{\gamma_1} \ln\left(1-\gamma_1\right) \\ &\quad \left. - \ln\left(\frac{1+\sqrt{1-\tau}}{2}\right) \ln\left(\frac{1-\sqrt{1-\tau}}{2}\right)\right] \\ &= \frac{1}{s}\left[-\frac{\pi^2}{2} + \frac{1}{2}\ln^2\left(\frac{1+\sqrt{1-\tau}}{2}\right) \pm i\pi \ln\left(\frac{1+\sqrt{1-\tau}}{2}\right)\right. \\ &\quad + \frac{1}{2}\ln^2\left(\frac{1-\sqrt{1-\tau}}{2}\right) \pm i\pi \ln\left(\frac{1-\sqrt{1-\tau}}{2}\right) \\ &\quad - \int_1^{(1+\sqrt{1-\tau})/2} \frac{d\gamma_1}{\gamma_1} \ln\left(1-\gamma_1\right) + \int_1^{(1+\sqrt{1+\tau})/2} \frac{d\gamma_1}{\gamma_1} \ln\left(1-\gamma_1\right) \\ &\quad \left. - \ln\left(\frac{1+\sqrt{1-\tau}}{2}\right) \ln\left(\frac{1-\sqrt{1-\tau}}{2}\right)\right]. \end{aligned} \tag{37}$$

We see that the remaining integrals (generating Spence functions) cancel.

Now use

$$(\ln(-a))^2 + (\ln(-b))^2 - 2\ln(a)\ln(b) \;=\; \left(\ln\left(\frac{a}{b}\right)\right)^2 - 2\pi^2 - i\pi\ln\left(\frac{a}{b}\right) \tag{38}$$

where the branch of the logarithm for negative argument is chosen to give a negative imaginary part (again, the amplitude then has a positive imaginary part as required by unitarity).

Finally, we have

$$C_0 \;=\; \frac{1}{2s}\left[\ln\left(\frac{1+\sqrt{1-\tau}}{1-\sqrt{1-\tau}}\right) - i\pi\right]^2. \tag{39}$$

Below threshold where $\tau > 1$ we make the substitution

$$\ln\left(\frac{1+\sqrt{1-\tau}}{1-\sqrt{1-\tau}}\right) - i\pi \;\rightarrow\; 2i\tan^{-1}\left(\frac{1}{\sqrt{\tau-1}}\right) \;=\; 2i\sin^{-1}\left(\frac{1}{\sqrt{\tau}}\right). \tag{40}$$

Similarly, start from

$$B_0(s,m^2) \;\equiv \frac{d^nk}{\pi^{n/2}}\frac{1}{(k^2-m^2)((k+p_1+p_2)^2-m^2)} + \frac{1}{(n-4)}(m^2)^{-(n-4)}. \tag{41}$$

Introducing Feynman parameters and shifting k to $k+\alpha(p_1+p_2)$, one gets

$$B_0(s,m^2) \;= \frac{d^nk}{pi^{n/2}}\int_0^1 d\alpha \frac{1}{\left[(k^2-m^2+s\alpha(1-\alpha)\right]^2} + \frac{1}{(n-4)}(m^2)^{-(n-4)}. \tag{42}$$

Performing the loop integral and cancelling the poles from the two terms gives

$$B_0 \;=\; -\int_0^1 d\alpha \ln\left(1 - \frac{s\alpha(1-\alpha)}{m^2}\right). \tag{43}$$

Again, setting $\tau = 4m^2/s$ and factorising the argument of the logarithm, we have

$$B_0 \;=\; -\int_0^1 d\alpha\left[\ln\left(1-\frac{2\alpha}{1+\sqrt{1-\tau}}\right) + \ln\left(1-\frac{2\alpha}{1-\sqrt{1-\tau}}\right)\right].$$

Integrating over α

$$\begin{aligned} B_0 \;&=\; 2 - \frac{1+\sqrt{1-\tau}}{2}\left(1-\frac{2}{1+\sqrt{1-\tau}}\right)\ln\left(1\frac{2}{1+\sqrt{1-\tau}}\right) \\ &\quad -\frac{1-\sqrt{1-\tau}}{2}\left(1-\frac{2}{1-\sqrt{1-\tau}}\right)\ln\left(1\frac{2}{1-\sqrt{1-\tau}}\right) \\ &=\; 2 - \sqrt{1-\tau}\ln\left(\frac{(1+\sqrt{1-\tau})}{(\sqrt{1-\tau}-1)}\right). \end{aligned}$$

Again if $\tau > 1$ we make the replacement

$$\ln\left(\frac{(1+\sqrt{1-\tau})}{(\sqrt{1-\tau}-1)}\right) \;\rightarrow\; 2i\sin^{-1}\left(\frac{1}{\sqrt{\tau}}\right). \tag{44}$$

The expressions obtained for the B_0 and C_0 scalar integrals correspond to well known expressions used in the case of a pseudoscalar Higgs boson entering $gg \to A \to \gamma\gamma$: practitioners would have recognised them.